ChemPubSoc Europe

DOI: 10.1002/chem.201406573

CHEMISTRY A European Journal Full Paper

Photochromism

Photochromism Emergence in *N*-Salicylidene *p*-Aminobenzenesulfonate Diallylammonium Salts

Pierre-Loïc Jacquemin, Koen Robeyns, Michel Devillers,* and Yann Garcia*[a]

Abstract: *N*-Salicylidene *p*-aminobenzenesulfonate salts were prepared by in situ condensation of *p*-aminobenzenesulfonate diallylammonium salt and salicylaldehyde. Modulation of thermo- and photochromism was achieved by varying the alkyl chain length of the diallylammonium countercation. A structural–optical properties investigation reveals that both crystal packing and dihedral angle between aromatic rings of the *N*-salicylidene aniline switch are not sufficient to predict the occurrence of photochromism in the solid state. The available free space around the *N*-salicylidene *p*-aminobenzenesulfonate, in addition to the flexibility of the nearby environment, is shown to be of major importance for the *cis*→*trans* isomerisation to occur as well as for the stabilisation of the *trans*-keto form. Emergence of photochromic properties was determined from the diallylhexylammonium cation within the series of investigated counter-cations. High stability is observed for the *trans*-keto form of one polymorph of *N*-salicylidene *p*-aminobenzenesulfonate diallylhexylammonium salt ($k = 2.4 \times 10^{-7}\ s^{-1}$).

Introduction

Photochromic molecules can find numerous applications of various nature, for instance in optical data storage and display devices,[1] photo-pharmacology,[2] sensors[3] and molecular rotors.[4] Major efforts have focused on diarylethenes[1c] and spiropyrazines,[1c] but little attention was devoted to *N*-salicylidene aniline derivatives (anils).[5] These molecules are an important substance class, which can present both solid-state thermo- and photochromism with different colours due to the presence of prototropic and isomeric forms.[5] Since their discovery, special focus was given to the determination of relationships between structural and optical properties to understand the mechanisms involved in their switching phenomenon occurring in the solid state.[6] Firstly, a thermal tautomeric equilibrium was identified between the yellow *cis*-keto form at room temperature and the white enol form at lower temperature to account for their thermochromism.[5] This equilibrium is effective when the alcohol group of the enol form is hydrogen bonded to the imine of the anil (Scheme 1). Secondly, a photo-isomerisation between the yellow *cis*-keto form and the red *trans*-keto form is induced by irradiating at $\lambda = 365$ or 450 nm.[5] The resulting *trans*-keto form usually relaxes back thermally to the *cis*-keto form but the reverse switching is also possible by irradiating at $\lambda = 545$ nm (Scheme 1).

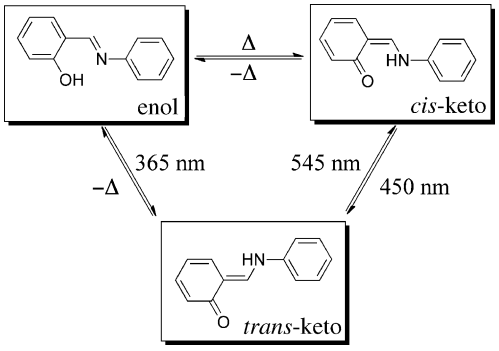

Scheme 1. Thermochromism and photochromism pathways of *N*-salicylidene aniline derivatives.

Two main structural factors to account for the *cis*–*trans* photo-isomerisation were defined: the planar character of the anil molecule and the crystal packing.[7] The planar character of the anil molecule is evaluated by the determination of the dihedral angle Φ between phenolic and benzene rings, which is effective when $\Phi < 25^\circ$. Twisted molecules ($\Phi > 25^\circ$) present an intramolecular hydrogen bond weaker than in planar molecules, which favours the photo-isomerisation. With a dense crystal packing, thermochromism is the solely observed phenomenon as the *cis*–*trans* isomerisation is prevented due to steric hindrance when rotating half of the molecule. In contrast, photochromism is observed for "open" crystal packings.[5c,d,7] Recent studies have, however, shown the limit of these structural considerations with the need to consider electronic effects.[8] In particular, the study of *N*-salicylidene aminopyridine derivatives revealed that molecules presenting a dense crystal packing and a planar character can display

[a] P.-L. Jacquemin, Dr. K. Robeyns, Prof. Dr. M. Devillers, Prof. Dr. Y. Garcia
Institute of Condensed Matter and Nanosciences
Molecules, Solids and Reactivity (IMCN/MOST)
Université Catholique de Louvain
Place L. Pasteur 1, 1348 Louvain-la-Neuve (Belgium)
Fax: (+32) 1047-2330
E-mail: michel.devillers@uclouvain.be
yann.garcia@uclouvain.be

Supporting information for this article is available on the WWW under http://dx.doi.org/10.1002/chem.201406573.

photochromism too, along with molecules in "open" structures displaying exclusively thermochromism.[8a] Most interestingly, the study of *N*-salicylidene aminomethylpyridines revealed the presence of the *trans*-keto form in non-photochromic species.[8b]

The modification of the direct environment of anil molecules is another way to modify their optical properties, in particular photochromism. Indeed, the insertion of neutral *N*-salicylidene aniline derivatives inside various host matrices (mesoporous silica,[9–11] polymers,[12,13] cyclodextrins)[14] could modulate the photochromic property and even induce it, as observed inside clathrates[15,16] and zeolites,[17,18] after modification of the dihedral angle (Φ). The inclusion of anil inside zeolites also modified the polarity of the medium allowing the formation of zwitterions, which change the photochemical pathway of formation of the *trans*-keto form.[17]

These methods suffer from lack of control of the number of guest molecules included, contrary to the entrapment of anils into molecular capsules,[19] as well as the functionalisation of these molecules as ligands for coordination complexes.[8a,20–22] Anionic derivatisation of anils constitutes an alternative for a controlled incorporation into positively charged matrices,[13,23,24] and in particular coordination complexes.[23] A sulfonate group was selected because of its permanent charge and low coordination ability, and deprotonation of the enol form was avoided to prevent any Schiff base coordination competition with transition metals. $[M(phen)_3]^{2+}$ (M = Cu, Ni; phen = 1,10-phenanthroline) was chosen as a template to successfully crystallise *N*-salicylidene aminobenzenesulfonate as counter-anions. These hybrid molecules present a tautomeric equilibrium after insertion, despite their exclusive thermochromic properties.[23b] A keto–enol equilibrium was also detected for *N*-salicylidene aminobenzenesulfonate inserted in Fe^{II}-1,2,4-triazole trinuclear complexes displaying thermo-induced spin crossover.[23a]

Herein, we present the first examples of photochromic *N*-salicylidene aminobenzenesulfonate anions, which were previously regarded as exclusively thermochromic.[13,23] Substituted diallylammonium derivatives as counter-cations were selected after functionalisation of the amine moiety (Scheme 2), thus allowing study of the effect of the alkyl chain length of the counter-cation on the optical properties of *N*-salicylidene *para*-aminobenzenesulfonate salts. The limit of the structural–optical properties model to predict the occurrence of photochromism in anil molecules is discussed with a focus on the available free space around the molecular switch, in addition to the flexibility of the nearby environment. A preliminary account of the optical properties of one salt (**3a**) is also communicated.[25]

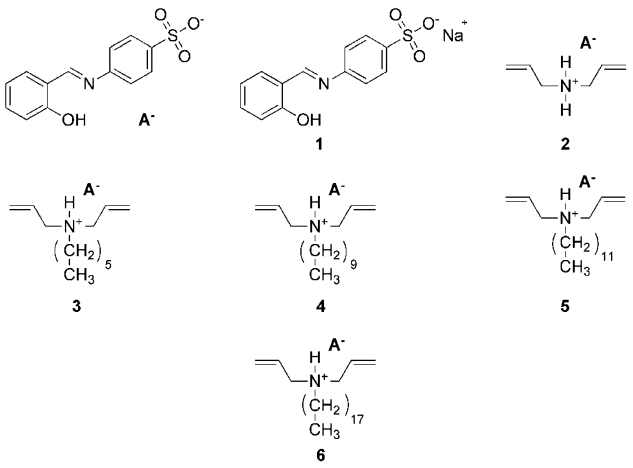

Scheme 2. The anions and diallylammonium derivatives used in the present work.

Results

Synthesis and crystallisation

The synthesis of *N*-salicylidene *p*-aminobenzenesulfonate sodium salt (**1**)[23b] was adapted to yield *N*-salicylidene *p*-aminobenzenesulfonate-substituted diallylammonium salts (**2**–**6**) in large amounts, to ease further characterisation of the optical properties. The first synthetic step concerns the deprotonation of sulfanilic acid by a substituted diallylamine. The resulting salt is then added to a methanolic solution of salicylaldehyde for the condensation into *N*-salicylidene *para*-aminobenzenesulfonate (Scheme 3). Diallylammonium salts were successfully purified by recrystallisation, as could be concluded from elemental analysis and ^{1}H NMR spectroscopy.

Slow evaporation of a methanolic solution of **1** at room temperature afforded long yellow needles, after 6 months, which were found suitable for X-ray data collection. Compounds **2**, **4**, **5** and **6** were crystallised from cold methanol at 253 K over one night as yellow needles. Orange needles were obtained for **3** by using the same conditions (**3a**), whereas yellow needles were crystallised by slow evaporation in darkness at room temperature (**3b**).

Structural studies

Crystal structure of sodium *N*-salicylidene *p*-aminobenzenesulfonate (1): Compound **1**·H_2O·MeOH crystallises in a monoclinic space group $P2_1/c$ (Table S1 in the Supporting Information). The structure can be seen as a two-dimensional network in which sodium atoms are linked by bridging water and methanol molecules or by a bidentate bridging sulfonate group (Na21—O2 and Na21—O3, respectively 2.356(2) and 2.399(2) Å; Figure 1). Each sodium centre sits in a slightly distorted octahedral coordination sphere (distortion parameter

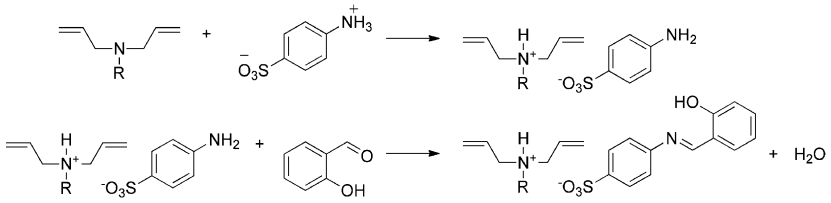

Scheme 3. Synthesis of the substituted diallylammonium salt of *N*-salicylidene *para*-aminobenzenesulfonate.

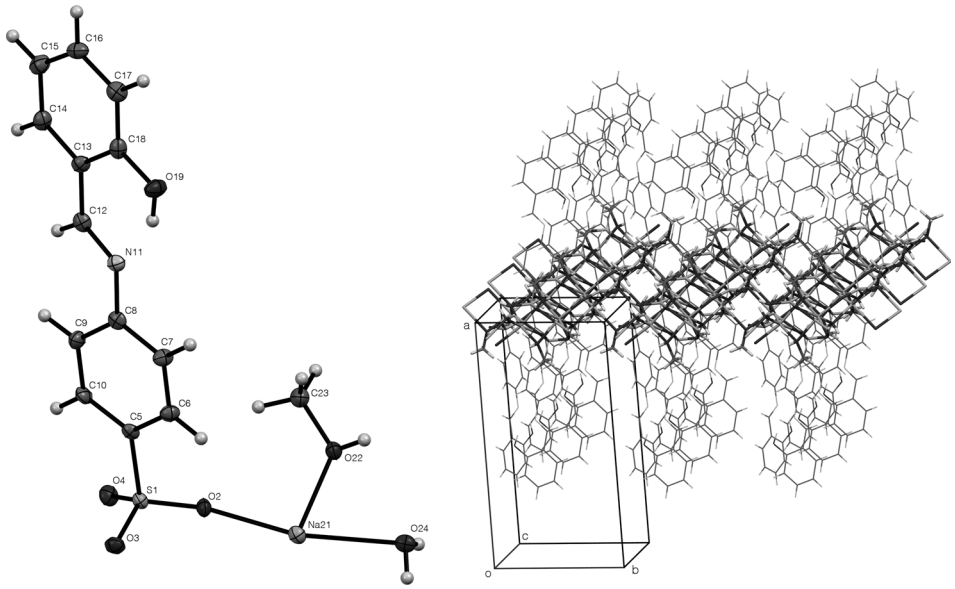

Figure 1. Left: ORTEP view of the asymmetric part of the unit cell of **1**·H_2O·MeOH, showing displacement ellipsoids at the 50% probability level. Right: Crystal packing projection of **1** along the *a* axis showing the 2D coordination network.

$\Sigma = 97(1)^\circ$[26] (Figure 2). The anil molecule is planar with a dihedral angle between two aromatic rings lower than 25° ($\Phi = 9.59(14)^\circ$). The planarity of the molecule is confirmed by the three torsion angles Γ_1, Γ_2 and Γ_3 (respectively $-10.6(4)$, 180.0(2) and $-2.7(4)^\circ$; Table S5 in the Supporting Information).

The dense crystal packing results from three intermolecular hydrogen bonds at 1.99(4), 2.08(3) and 2.12(3) Å (Table S3 in the Supporting Information) and two additional T-shaped C–H···π interactions that include aromatic rings at 2.83 and 2.88 Å (C–H(H) centroid distance). The enol and imine functions are not involved in intermolecular hydrogen bonds and therefore allow the thermal keto–enol equilibrium.

Crystal structure of diallylammonium *N*-salicylidene *p*-aminobenzenesulfonate (2): Compound **2** crystallises in the orthorhombic space group *Pbcn* (Table S1 in the Supporting Information). The asymmetric unit of the cell presents two diallylammonium cations and two anil sulfonate anions in their enol form (Tables S2 and S4 in the Supporting Information; Figure 3).

Both anils are twisted with regard to the dihedral angles between their aromatic rings. The dihedral angle of anion 1 is

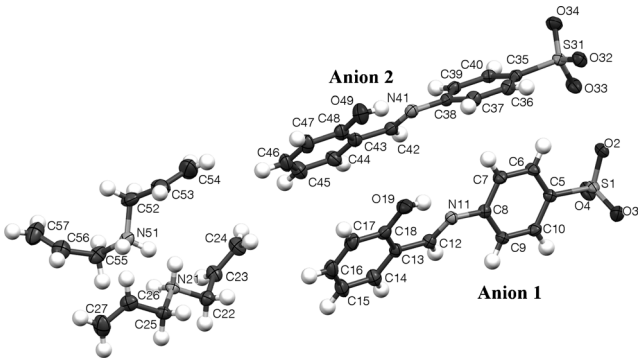

Figure 3. ORTEP view of the asymmetric part of the unit cell of **2**, showing displacement ellipsoids at the 50% probability level.

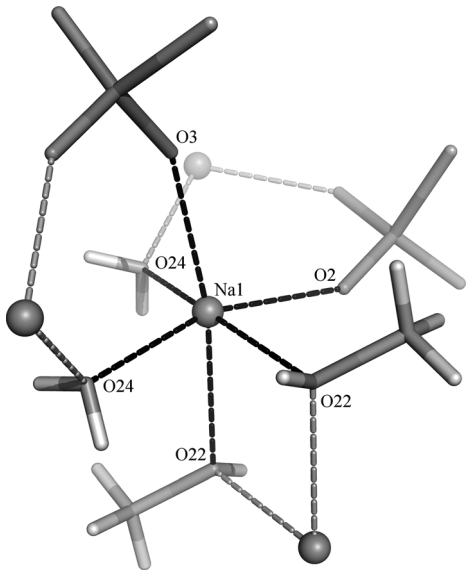

Figure 2. View of the octahedral coordination sphere of Na, formed by two water molecules, two methanol molecules and two sulfonate groups of the anions, within the crystal packing of **1**·H_2O·MeOH.

$\Phi_1 = 26.29(12)^\circ$. The twisting of this anion is also observed through torsion angles Γ_1, Γ_2 and Γ_3 ($-30.3(3)$, 177.4(2), 3.5(4)°, respectively). Anion 2 is even more twisted than anion 1 with a dihedral angle between aromatic rings of $\Phi_2 = 34.95(12)^\circ$ (torsion angles: Γ_4, Γ_5 and Γ_6 of 35.6(3), $-178.8(2)$ and $-0.3(4)^\circ$, respectively).

The crystal structure of **2** is organised by intermolecular interactions (Table S3 in the Supporting Information). Contrary to **1**, there is no coordination of the cation to oxygen atoms.

Crystal structure of diallylhexylammonium *N*-salicylidene *p*-aminobenzenesulfonate (3): The crystal structure of **3a** presents one diallylhexylammonium cation and one *N*-salicylidene *para*-aminobenzenesulfonate in the monoclinic $P2_1$ space group (Figure 4). With its dihedral angle Φ of 17.69(12)°, *N*-salicylidene *p*-aminobenzenesulfonate can be considered as nearly planar. The planarity of the molecule is also confirmed through the three torsion angles Γ_1, Γ_2 and Γ_3 (respectively 17.8(4),

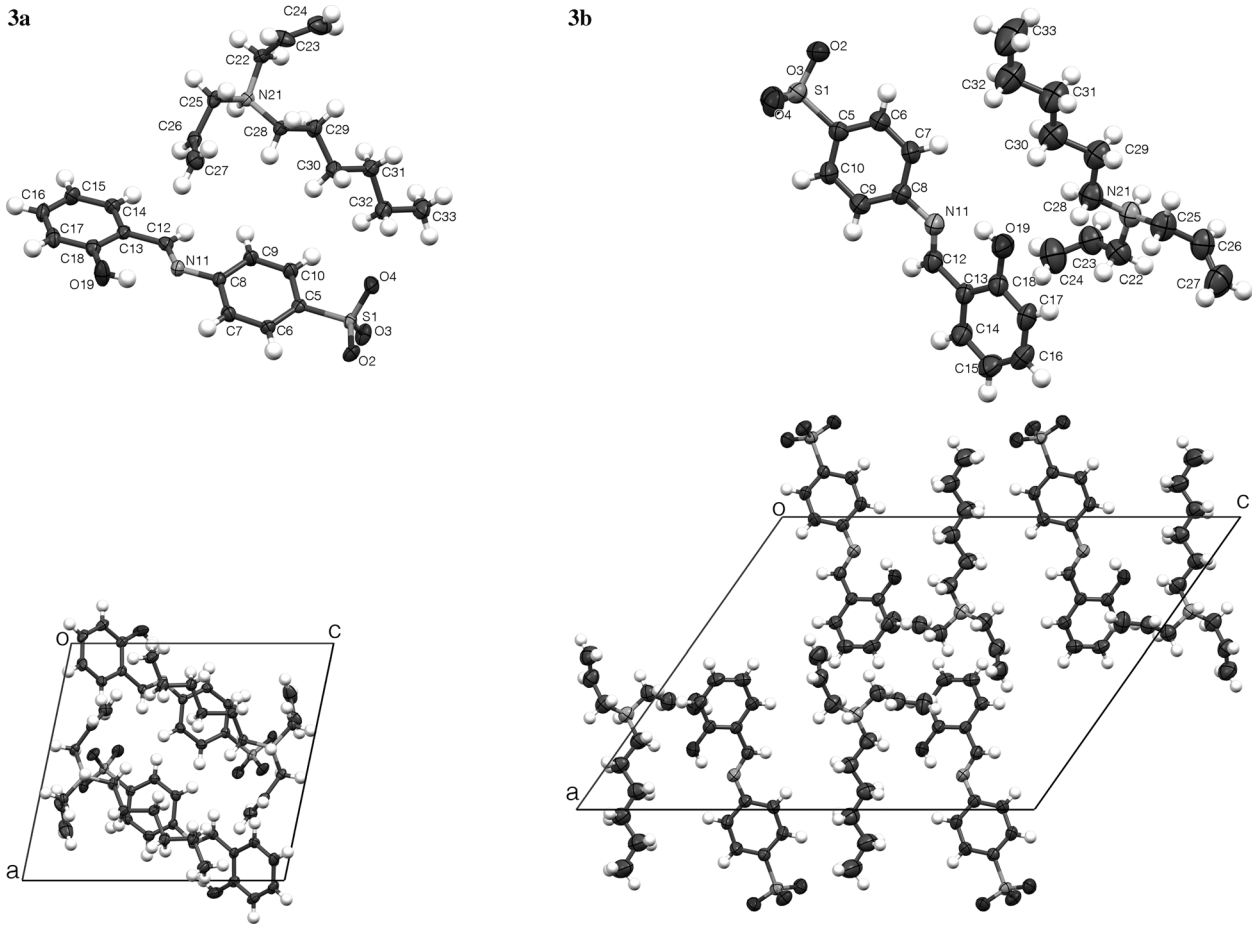

Figure 4. Top: ORTEP view of the asymmetric part of the unit cell of **3a** and **3b**, showing displacement ellipsoids at the 50% probability level. Bottom: Comparison of the crystal packings along the *b* axis.

178.8(2) and −1.0(4)°). The crystal packing presents two intermolecular hydrogen bonds at 1.98(1) and 2.51(1) Å (Table S3 in the Supporting Information), as well as various closed contacts and can be regarded as "open" according to the Hadjoudis classification.[7]

Compound **3b** crystallises in the monoclinic space group $P2_1/c$. One diallylhexylammonium cation and one anil anion are observed in the asymmetric part of the unit cell (Figure 4). The anion is twisted with regard to the dihedral angle between aromatic rings of 25.39(11)°, as well as torsion angles of Γ_1, Γ_2 and Γ_3 (respectively 21(1), −172(1) and −1 (1)°).

Compound **3b** presents only one strong intermolecular hydrogen bond, contrary to **3a**, which presents two intermolecular hydrogen bonds (Table S4 in the Supporting Information).

Crystal structure of diallyldecylammonium *N*-salicylidene *p*-aminobenzenesulfonate (4): Compound **4** crystallises in the monoclinic space group *Cc*. Three diallyldecylammonium cations in addition to three anil anions are observed in the asymmetric part of the unit cell (Figure 5). Anion 1 is slightly twisted with a dihedral angle between aromatic rings $\Phi_1 = 23.28(13)°$, which is confirmed by inspecting torsion angles Γ_1, Γ_2 and Γ_3 (−23.9(6), −179.0(3) and 0.2(6)(1)°, respectively). The same dihedral angle between aromatic rings as for anion 1 is measured in anion 2 ($\Phi_3 = 22.85(13)°$ and torsion angles: Γ_7, Γ_8 and Γ_9 of −23.7(4), 178(3) and 1.3(6)°, respectively). Anion 3 is slightly more twisted with a dihedral angle between aromatic rings $\Phi_4 = 25.71(13)°$ (torsion angles Γ_{10}, Γ_{11} and Γ_{12}: −24.3(4), 178.1(3) and 1.0(5)°, respectively). Six intermolecular hydrogen

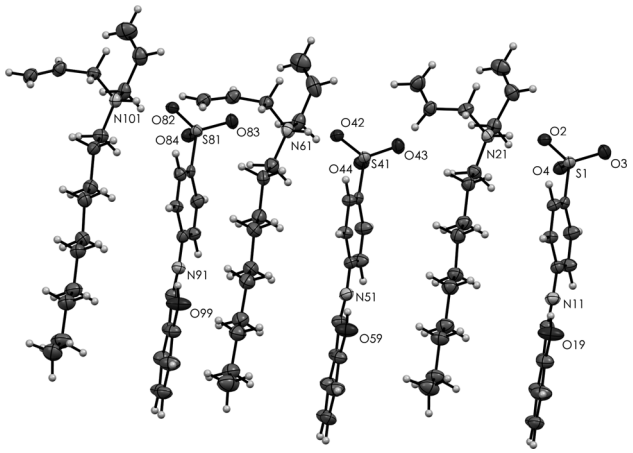

Figure 5. ORTEP view of the asymmetric part of the unit cell of **4**, showing 50% probability displacement ellipsoids; carbon atom labels are omitted for clarity.

bonds are observed between the molecules (Table S3 in the Supporting Information), which lead to a highly organised crystal structure. The C18–O19 and N11–C12 distances are shorter in the anions of **4** than in other compounds (Table S4 in the Supporting Information). Nonetheless, the distances relative to the intramolecular hydrogen bonds (Table S3 in the Supporting Information) indicate that the enol form is mainly observed in the crystal structure of **4**.

Crystal structure of diallyldodecylammonium *N*-salicylidene *p*-aminobenzenesulfonate (5): The crystal structure of **5** (monoclinic space group $P2_1/c$) reveals one *N*-salicylidene *p*-aminobenzenesulfonate anion, one diallyldodecylammonium cation and one MeOH molecule in the asymmetric part (Figure 6). The

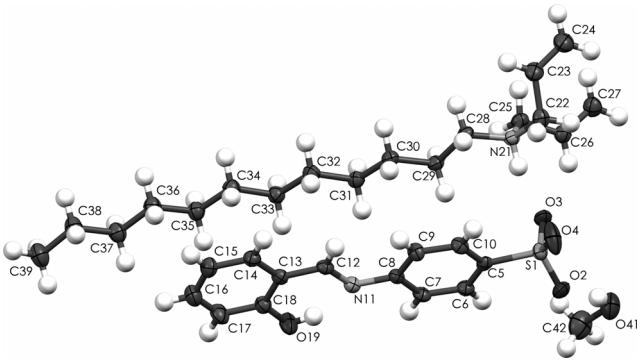

Figure 6. ORTEP view of the asymmetric part of the unit cell of **5**, showing displacement ellipsoids at the 50% probability level.

anion is planar with a dihedral angle between aromatic rings $\Phi_1 = 4.80(15)^\circ$, the planar character being confirmed by torsion angles Γ_1, Γ_2 and Γ_3 of 6.3(1), −177.9(6) and −2.7(1)°, respectively. Non-coordinated methanol is trapped in the crystal packing through an intermolecular hydrogen bond and a second intermolecular hydrogen bond is observed between cations and anions (Table S3 in the Supporting Information).

Crystal structure of diallyloctadecylammonium *N*-salicylidene *p*-aminobenzenesulfonate (6): Compound **6**, which crystallises in the triclinic space group $P\bar{1}$, presents one diallyloctadecylammonium cation and one *N*-salicylidene *p*-aminobenzenesulfonate anion in the asymmetric unit (Figure 7). The anion

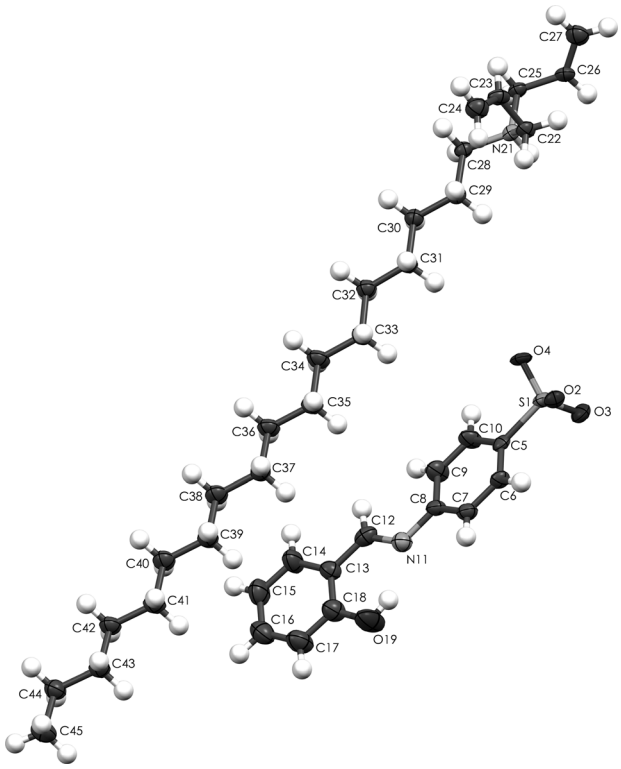

Figure 7. ORTEP view of the asymmetric part of the unit cell of **6**, showing displacement ellipsoids at the 50% probability level.

is almost planar with a dihedral angle between aromatic rings $\Phi_1 = 14.66(16)^\circ$. The planar character is also observed through torsion angles Γ_1, Γ_2 and Γ_3 of −14.7(1), −179.6(6) and 2.3(1)°, respectively. In addition, one strong intermolecular hydrogen bond is noticed between the cations and anions (Table S3 in the Supporting Information).

Optical properties

Thermochromic and photochromic phenomena in 1–6: All six compounds display thermochromism, from yellow at 298 K (*cis*-keto form) to white on cooling at 77 K (enol form; Figure 8). Exceptions were noticed for **3a** and **3b** for which a light orange colour is observed, which calls for the presence of the *trans*-keto form, which is interestingly stabilised without light irradiation at room temperature. Considering the series,

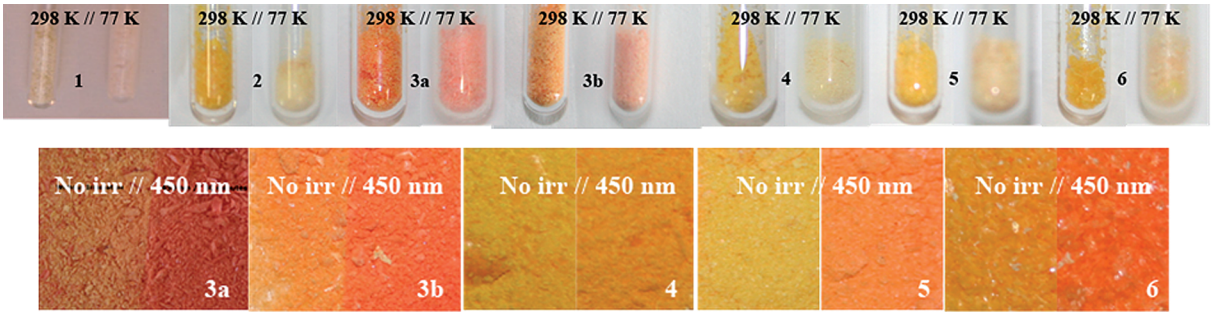

Figure 8. Photographs of tubes containing: top: **1**–**6** at 298 and 77 K; bottom: **3a** to **6** before and after irradiation at $\lambda = 450$ nm.

five compounds display photochromism in addition to their thermochromic properties (**3a** to **6**; Figure 8). Indeed, **1** and **2** do not show any modification of colour after irradiation, neither at $\lambda = 365$ nm nor at 450 nm. Photochromism is observed from yellow (**3b** to **6**) or yellow-orange (**3a**) before irradiation to orange after irradiation at $\lambda = 450$ nm during 30 min. The orange colour is due to the absorption of the *trans*-keto form. The colour change is strong for **3a**, **3b**, **5** and **6**, but weaker for **4** (Figure 8).

Diffuse reflectance spectroscopy: All compounds were analysed by diffuse reflectance spectroscopy (DRS) to confirm the presence of possible conformations of *N*-salicylidene aniline *p*-aminobenzenesulfonate derivatives (Figure 9). Three areas can be defined: the white enol form, which is usually observed below about 400 nm, the yellow *cis*-keto form between about 400 and 525 nm, and the red *trans*-keto form above approximately 525 nm.

For **1**, the enol form is the most representative but a weaker band is noticed between 400 and 500 nm corresponding to the *cis*-keto form, which explains the very light yellow colouration of **1** at 298 K (Figure 8).[23b] For **2**, the contribution of the *cis*-keto form is much more important, which is confirmed by the pronounced yellow colour at 298 K (Figure 8). Both diffuse reflectance spectra remain unchanged after irradiation at $\lambda =$ 450 nm during 20 min (Figure S1 in the Supporting Information). The *trans*-keto form was detected for both **3a** and **3b**. Interestingly, polymorphs **3a** and **3b** show remarkable photochromic properties accompanied by a *cis*–*trans* isomerisation

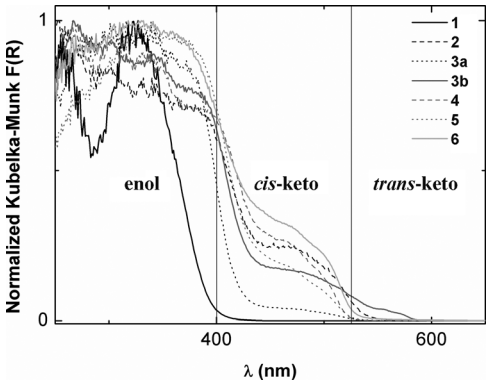

Figure 9. Comparison between diffuse reflectance spectra of **1**–**6**.

of the keto form under the same experimental conditions as for **2** (Figure 10), but a different relaxation behaviour for the *trans*-keto form is noticed (Figure 10). Indeed, for **3a**, only 12% of the *trans*-keto form is reverted back to the *cis*-keto form after 8000 min ($k_{3a} = 2.4 \times 10^{-7}$ s^{-1}) whereas 50% of the *trans*-keto form relaxed for **3b** ($k_{3b} = 2.2 \times 10^{-6}$ s^{-1}). The *trans*-keto form is thus less stable in **3b** than in **3a** ($k_{3b} > k_{3a}$).

The photo-reversibility of the *cis*–*trans* isomerisation of the keto form in **3a** and **3b** was confirmed by time-dependent measurements (Figure 11). The reflectance was measured at $\lambda = 550$ nm using irradiation cycles at $\lambda = 450$ nm during 30 min for the *cis*→*trans* isomerisation and at $\lambda = 546$ nm during 30 min for the reversible photoreaction.

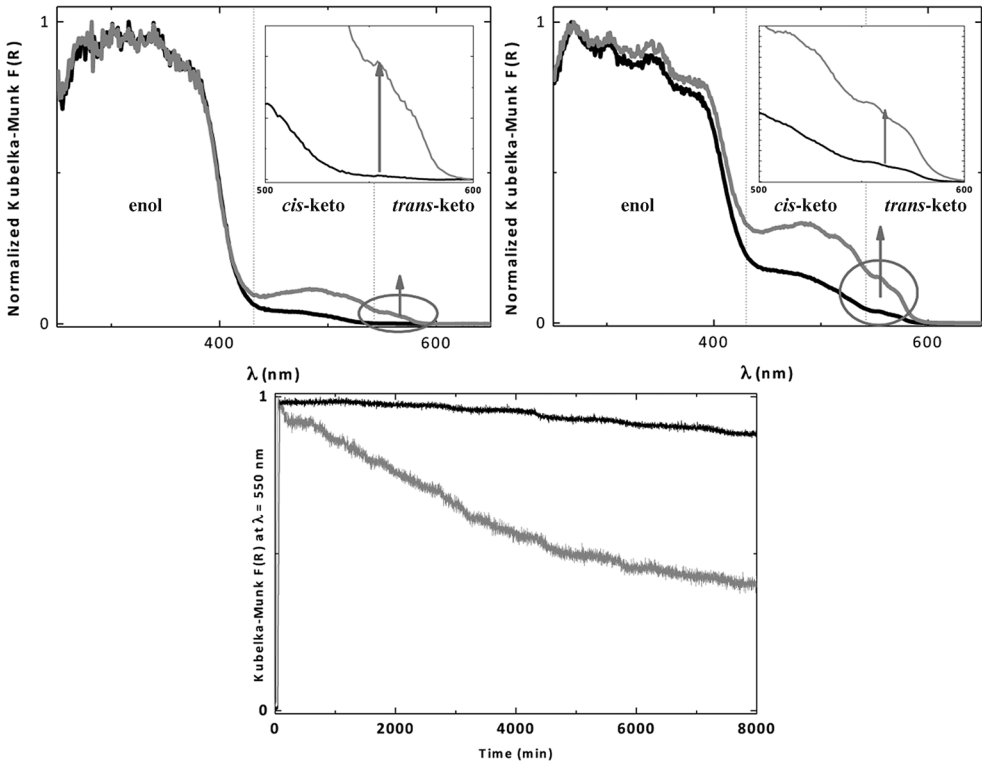

Figure 10. Top: Diffuse reflectance spectra of **3a** (left) and **3b** (right) before (black) and after (grey) irradiation at $\lambda = 450$ nm during 20 min. Circles highlight the increase of *trans*-keto contribution, as shown in the inset. Bottom: Time dependence of the Kubelka–Munk function of **3a** (black) and **3b** (grey) at $\lambda = 550$ nm showing thermal relaxation after light irradiation.

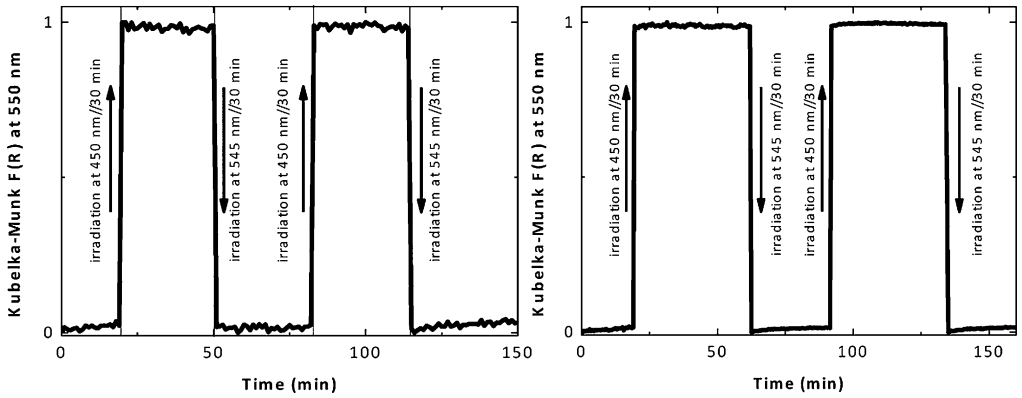

Figure 11. Time dependence of the Kubelka–Munk function of **3a** (left) and **3b** (right) at $\lambda = 550$ nm showing the reversibility of the *cis–trans* isomerisation with irradiation cycles at $\lambda = 450$ and 545 nm.

Upon irradiation, **4** and **5** show a slight increase of a new band above 520 nm corresponding to the contribution of the *trans*-keto form (Figure 12). This form is much less stable than for **3a** and **3b** as concluded from time-dependent measurements (Figure 13). Indeed, the *trans*-keto form is completely relaxed after 100 min for **4** ($k = 6.7 \times 10^{-4}\ s^{-1}$) and 120 min for **5** ($k = 4.7 \times 10^{-4}\ s^{-1}$).

Photo-reversibility was checked by time-dependent measurements using photo-cycles at 450 nm during 30 min for the *cis*→*trans* isomerisation and at 545 nm for the back formation of the *cis*-keto form (Figure 13). Interestingly, after irradiation at $\lambda = 545$ nm, the intensity of the band at 550 nm increases slowly, thus indicating that the *trans*-keto is re-formed. A similar phenomenon, although more pronounced, was observed for *N*-salicylidene-4-amino-3,5-bis(pyridine-2-yl)-1,2,4-triazole, which was attributed to the formation of a cyclised intermediate predicted by computational means (spring-type effect[20]). For **4** and **5**, the back reaction may be explained by a resistance of the surrounding of the anion to the isomerisation, packed in the crystal lattice. The *trans*-keto form is then regenerated after the forced formation of a *cis*-keto form.

The last compound **6** also displays photochromism, which was observed in the DRS spectra, with the rising of a new band above 520 nm as a result of the *trans*-keto form popula-

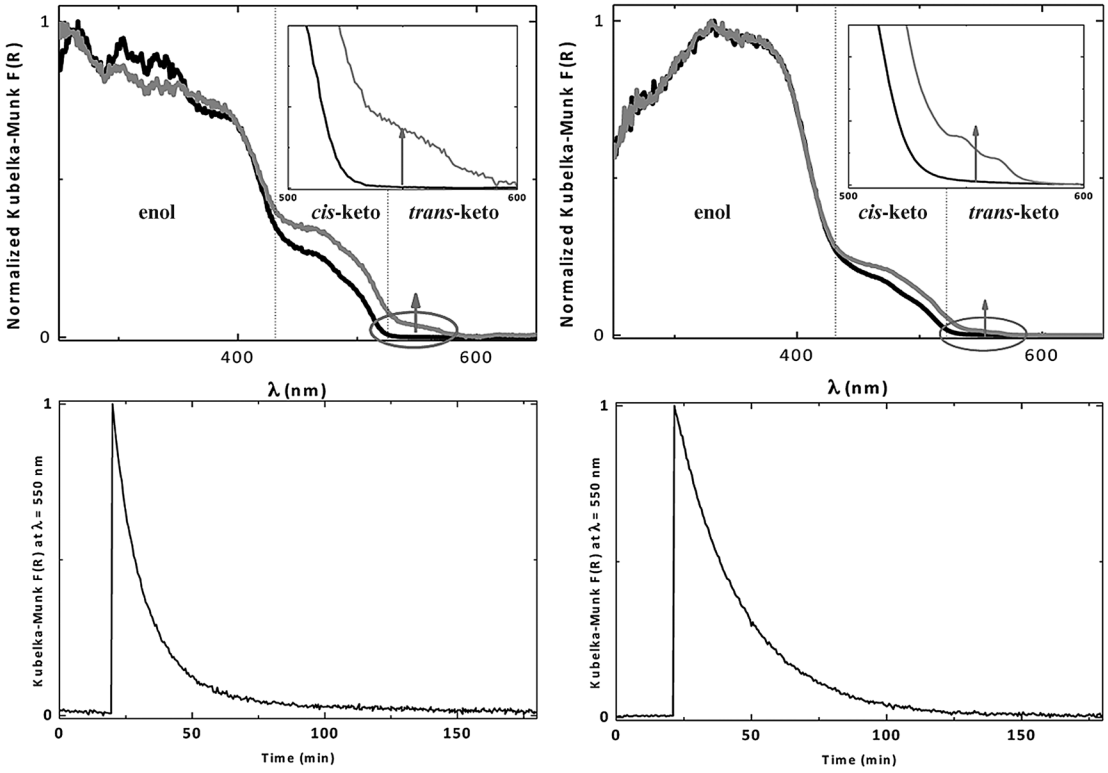

Figure 12. Top: Diffuse reflectance spectra of **4** (left) and **5** (right) before (black) and after (grey) irradiation at $\lambda = 450$ nm during 20 min. Circles highlight the increasing *trans*-keto contribution. Bottom: Time dependence of the Kubelka–Munk function of **4** (left) and **5** (right) at 550 nm showing thermal relaxation after irradiation at $\lambda = 450$ nm during 20 min.

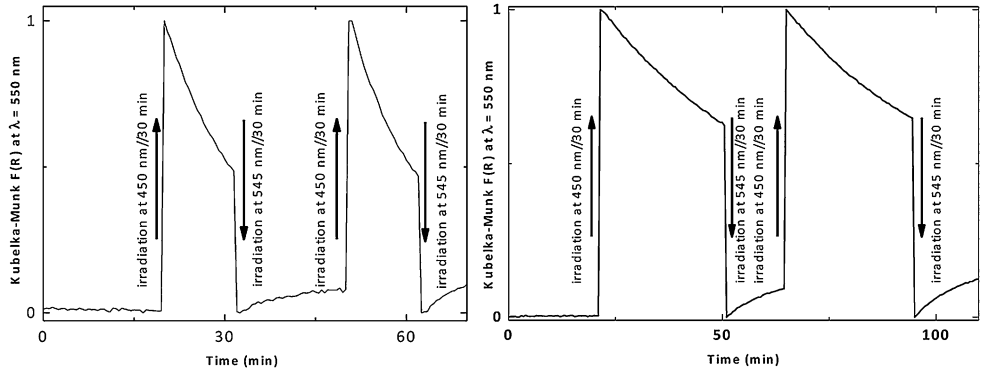

Figure 13. Time dependence of the Kubelka–Munk function of **4** (left) and **5** (right) at 550 nm showing the reversibility of the *cis–trans* isomerisation with irradiation cycles at 450 and 545 nm.

tion (Figure 14). The thermal stability of this form, recorded by time-dependent DRS, shows its full disappearance after 7000 min ($k = 1.1 \times 10^{-5}\ s^{-1}$). The photo-reversibility of the *cis–trans* isomerisation was also demonstrated (Figure 14). As noticed for **4** and **5**, a slight increase of the Kubelka–Munk function, due to the spontaneous formation of the *trans*-keto form, is observed.

Solid-state fluorimetry: Crystals of the six compounds were analysed by solid-state fluorimetry to study the photochemical processes involved. In emission measurements, the excitation wavelength is locked on a selected area of the diffuse reflectance spectrum corresponding to the band maximum of the prototropic form of the *N*-salicylidene derivative to be analysed, and the emission wavelength is scanned.[8b] The spectrum contains all emissions driven from the generated excited form (e.g., irradiating at $\lambda^{exc} = 450$ nm leads to the enol* form and emissions of enol*→enol (A) and *cis*-keto*→*cis*-keto (B), as depicted in Scheme 4). In the excitation mode, the emission wavelength is fixed at its maximum and an excitation spectrum is scanned. For example, we shall focus hereafter on the *cis*-keto*→*cis*-keto emission at $\lambda^{em} = 540$ nm and scan excitation wavelengths. The excitation spectrum is expected to reveal two bands corresponding to pathways C (enol→enol*→*cis*-keto*) and D (*cis*-keto→ *cis*-keto*) leading to the formation of the monitored emitting excited state (Scheme 4).

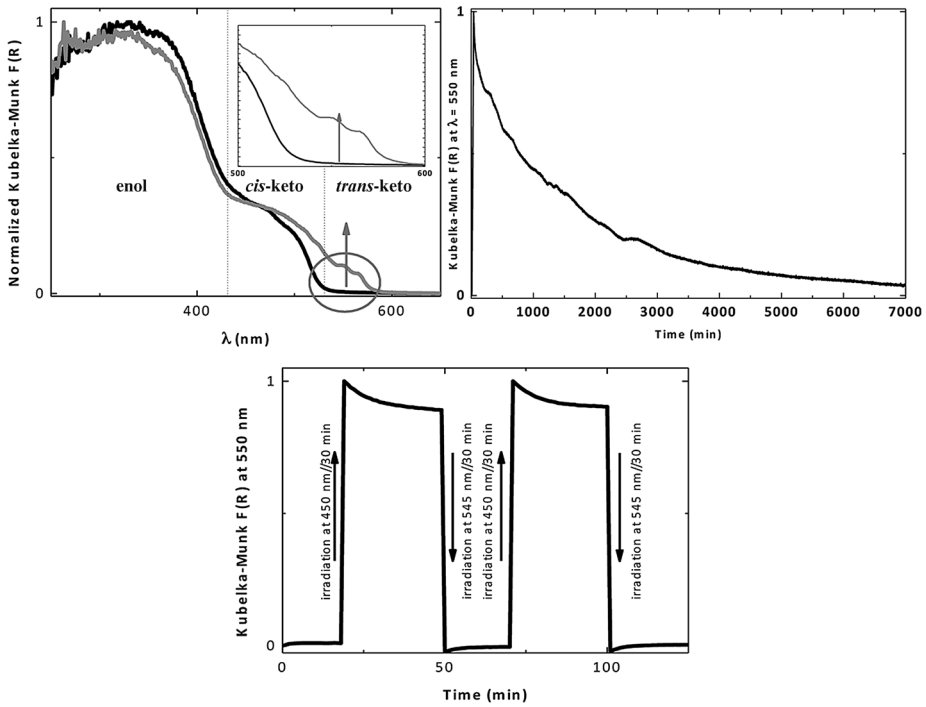

Figure 14. Top: Left: Diffuse reflectance spectra of **6** before (black) and after (grey) irradiation at 450 nm during 20 min. The circles highlight the increase of the *trans*-keto contribution. Right: Time dependence of the Kubelka–Munk function of **6** at 550 nm showing thermal relaxation after irradiation at 450 nm during 20 min. Bottom: Time dependence of the Kubelka–Munk function of **6** at $\lambda = 550$ nm showing the reversibility of the *cis–trans* isomerization with irradiation cycles at $\lambda = 450$ and 545 nm.

Molecules **1**–**6** were analysed using an excitation wavelength of $\lambda^{exc} = 450$ nm (Figure 15). The analysis of emission spectra shows that the fluorescence of *N*-salicylidene aniline sulfonate derivatives is similar, with differences observed for the polymorphs of **3**. As an example, **1** presents an emission maximum at 540 nm, which is due to the enol→enol* and *cis*-keto→*cis*-keto* formations, and another band at 660 nm, which is due to the radiative relaxation of the *trans*-keto* form. Such a *trans*-keto→*trans*-keto* transition was already observed in non-photochromic molecules of this substance class.[8b] For **2**, the emission maximum is recorded at 550 nm. Two major contributions are observed at 475 and 520 nm in the excitation spectrum at $\lambda^{exc} = 550$ nm.

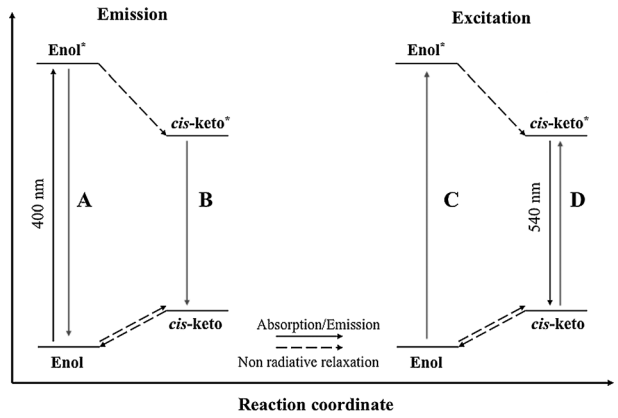

Scheme 4. Photochemical processes evidencing two radiative relaxation pathways in emission mode (A, B) and two absorption pathways in excitation mode (C, D) for the *N*-salicylidene aniline derivatives under consideration.

Discussion

The quest for *N*-salicylidene aniline derivatives that crystallise as single crystals is of major importance to determine optical–structural property relationships that will favour the crystal engineering of new materials with desired functional properties. In this context, we have prepared a series of crystals with various substituted diallylammonium counter-cations and *N*-salicylidene aniline sulfonate counter-anions. This approach contrasts with classic studies in which modifications were made either on the anil derivatives by chemical substitution[27,28] or on their immediate surroundings, for instance by inserting a switch into zeolites[17,18] or by dispersion into a given polymer,[13] ways that are less controllable than a direct electrostatic interaction as in the present case. Modifying the surroundings of *N*-salicylidene *p*-aminobenzenesulfonate is indeed expected to impact the optical properties of the molecular switch.

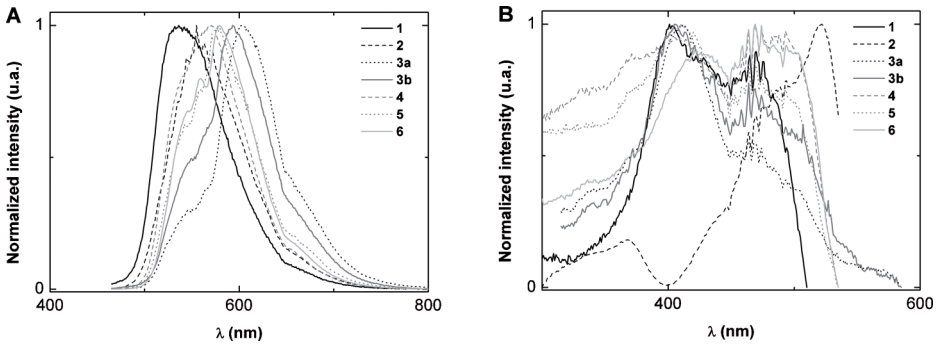

Figure 15. A) Emission spectra of solid samples of **1** to **6** ($\lambda^{exc}=450$ nm) at 298 K. B) Excitation spectra of solid samples of **1** ($\lambda^{em}=540$ nm), **2** ($\lambda^{em}=550$ nm), **3a**, **3b**, **4** and **6** ($\lambda^{em}=600$ nm), and **5** ($\lambda^{em}=580$ nm) at 298 K.

These contributions are due to the *cis*-keto→*cis*-keto* transition for the two anions present in the asymmetric part of the crystal structure (Figure 3). Two weak contributions are also noticed at 445 and 350 nm, which are due to the enol→enol* transitions for the same anions. The main emission band is observed at 600 nm for **3a** and **3b** with two other bands at 550 and 660 nm. Both polymorphs present the same three contributions in the excitation spectra ($\lambda^{exc}=600$ nm). The main contribution observed at 400 nm corresponds to the enol→enol* transition, the second (at 475 nm) is associated with the *cis*-keto→*cis*-keto* transition and a weak band is observed at 560 nm, which is due to the *trans*-keto→*trans*-keto* transition. For **3a** and **3b**, the presence of this particular transition may be due to the stabilisation of the *trans*-keto form in the ground state as observed in the DRS spectra (Figure 10). Compounds **4** and **6** present an emission maximum at 600 nm, which originates from the enol→enol* and *cis*-keto→*cis*-keto* transitions that are found at 400 and 500 nm, respectively, in the excitation spectra. No *trans*-keto→*trans*-keto* transition was detected in the excitation spectra. Finally, **5** presents an emission band at 580 nm. This emission is also due to the contributions of the enol→enol* and *cis*-keto→*cis*-keto* transitions (respectively at 400 and 500 nm).

Compounds **1**–**6** present thermochromism on cooling from room temperature, which was expected from the analysis of their crystal structures, which reveal an intramolecular hydrogen bond between the alcohol function and the amine moiety of the *N*-salicylidene *p*-aminobenzenesulfonate anion in its enol form (Tables S2 and S4 in the Supporting Information). This intramolecular hydrogen bond favours the tautomeric equilibrium between enol and *cis*-keto forms, and therefore the colour change. Prediction of the photochromic properties of anil derivatives is usually guaranteed by considering the distorted character of the switching molecule (with a dihedral angle between aromatic moieties $\Phi > 25^\circ$) and a crystal packing of "open"-type nature.[7] Several studies have, however, pointed out the limit of this structural prediction.[8,21,29] A similar situation is found in the present work. Indeed, although the prediction is confirmed for **2**, **3b** and **4**, which present an average dihedral angle higher than $\Phi > 25^\circ$ (35(1), 25(1) and 26(1)°, respectively; Figure 17), **2** is not photochromic. On the other hand, out of the planar molecules **1**, **3a**, **5** and **6**, all are photochromic except **1**. The latter situation is in agreement with the crystal packing prediction because this material presents an intermolecular distance (3.4 Å) with five stabilising interactions (three H-bonds and two C–H···π interactions), which qualifies this packing as "closed". "Open"-type structures are found for **2**–**6** with an intermolecular distance higher than 3.5 Å, but **2** is not photochromic. Considering such noticeable limitations to predict the optical properties of anils, the search for a more reliable tool was undertaken in the present work.

A significant trend was identified by comparing the size of the counter-cation of the anil derivatives containing a substituted diallylammonium group (**2**–**6**), evaluated through the pro-

jected length of the chain, with their optical properties. As expected, an overall increase of the length of the cation from 7.3 to 27.2 Å with the increase of lateral alkyl chain length is noticed, as a result of the linear character of diallylammonium salts (Figure 16). These lengths were compared to that of the *N*-salicylidene *p*-aminobenzenesulfonate anion with an average size of 12.3 Å.

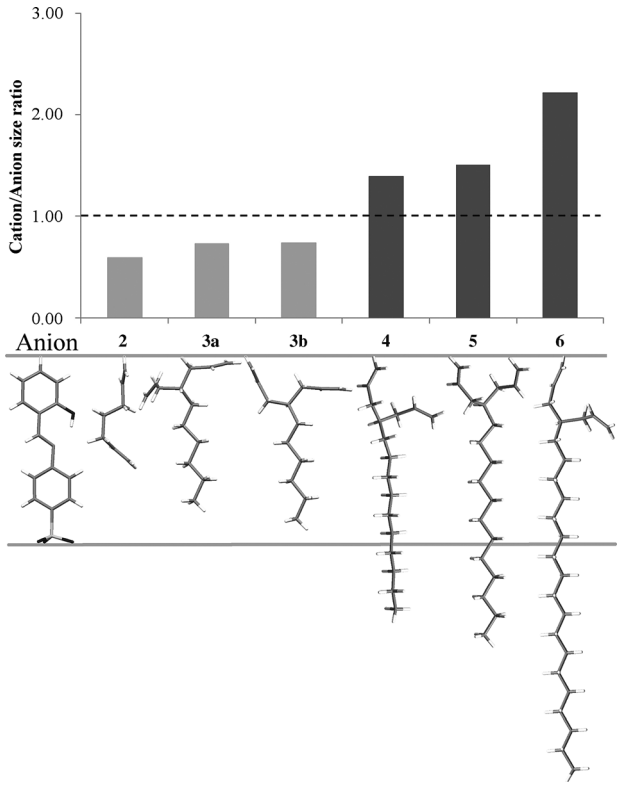

Figure 16. Top: Evolution of size of the diallylammonium cations relative to the size of the anion in **2**–**6**. All salts display thermochromism (depicted in light grey for **2**), whereas **3**–**6** display photochromism (dark grey bars). Bottom: Comparison between the size of diallylammonium cations **2**–**6** and the *N*-salicylidene *p*-aminobenzenesulfonate anion of 12.3 Å. The dotted line indicates a cation/anion ratio of one. The cation size of **4**–**6** clearly exceeds that of the anion.

Analysis of the crystal packing of **2** (Figure 17), **3a** and **3b** (Figure 4) reveals that flexible substituted diallylammonium cations are organised around the anions. A reverse situation is met when the size of the cation exceeds that of the anion as found for **4**–**6**. In this case, the anions are inserted between the cationic planes in a regular fashion. Actually, a transition is observed from a monolayer (for **4**) with a head-to-tail arrangement of molecules, to an intermediate situation (**5**) up to a bilayer one for **6**, with a head-to-head arrangement of molecules (Figure 17). Indeed, in each crystal structure, *N*-salicylidene *p*-aminobenzenesulfonate is parallel to the alkyl chain of the substituted diallylammonium unit and has its sulfonate moiety electrostatically linked to the ammonium part of the counterion. In the crystal packing of **4**–**6**, a segregation of the ionic part of the molecules is noticed leading to the separation of lipophilic domains. This separation is stronger for **6**, in which

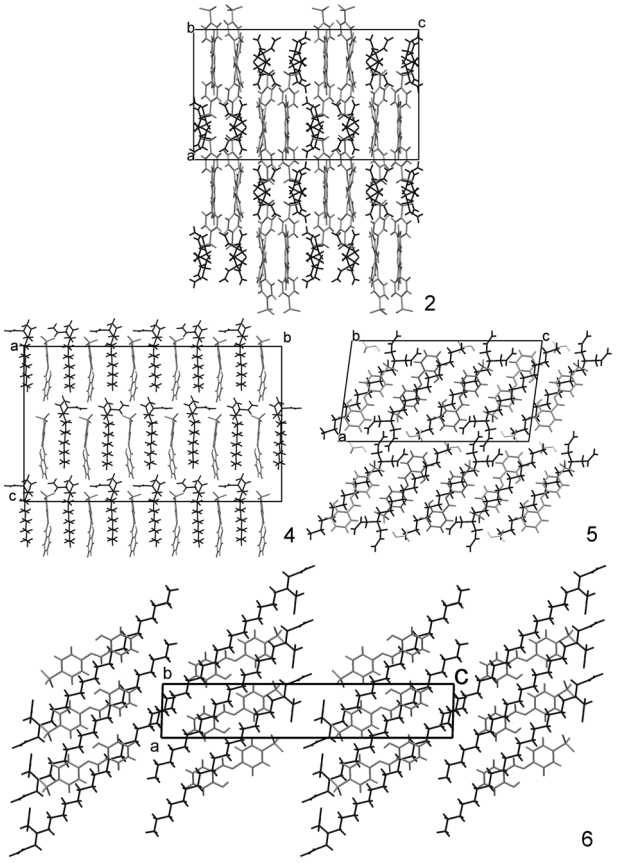

Figure 17. Comparison between the crystal packing of **2** (top), **4** and **5** (middle), and **6** (bottom). Anions are depicted in light grey and cations in dark grey.

a bilayer lamellar structure is observed with an inter-planar distance of 34.1 Å. Noticeably, a lamellar structure with an interchain distance of 32.5 Å was postulated from X-ray powder diffraction analysis of the copolymer synthesised from substituted diallylamine, that is, poly(*N*,*N*-diallyloctadecylamine-*alt*-maleic acid) ($CopoC_{18}H$).[30] We thus present the first indirect proof of this organisation, which was discussed in earlier works.[31,32]

Considering, as discussed above, the limit of the structural considerations to predict optical properties of *N*-salicylidene derivatives, we introduce the determination of the average free available space V_{free} around each switching molecule in the crystal lattice, as a complementary criterion. This free space is important because it allows the local rearrangement of molecules during the *cis*–*trans* isomerisation, thereby provoking photochromism. The free volume V_{free} was evaluated by considering the unit cell volume, the anion and cations volumes as well as *Z*, the number of molecules in the unit cell [Eq. (1)]:

$$V_{free} = \frac{V_{unit\,cell} - Z \times (V_{anion} + V_{cation})}{Z} \quad (1)$$

The anion and cation volumes were evaluated using the Molinspiration platform based on group contributions.[33] By considering the free volume, we determined that photochrom-

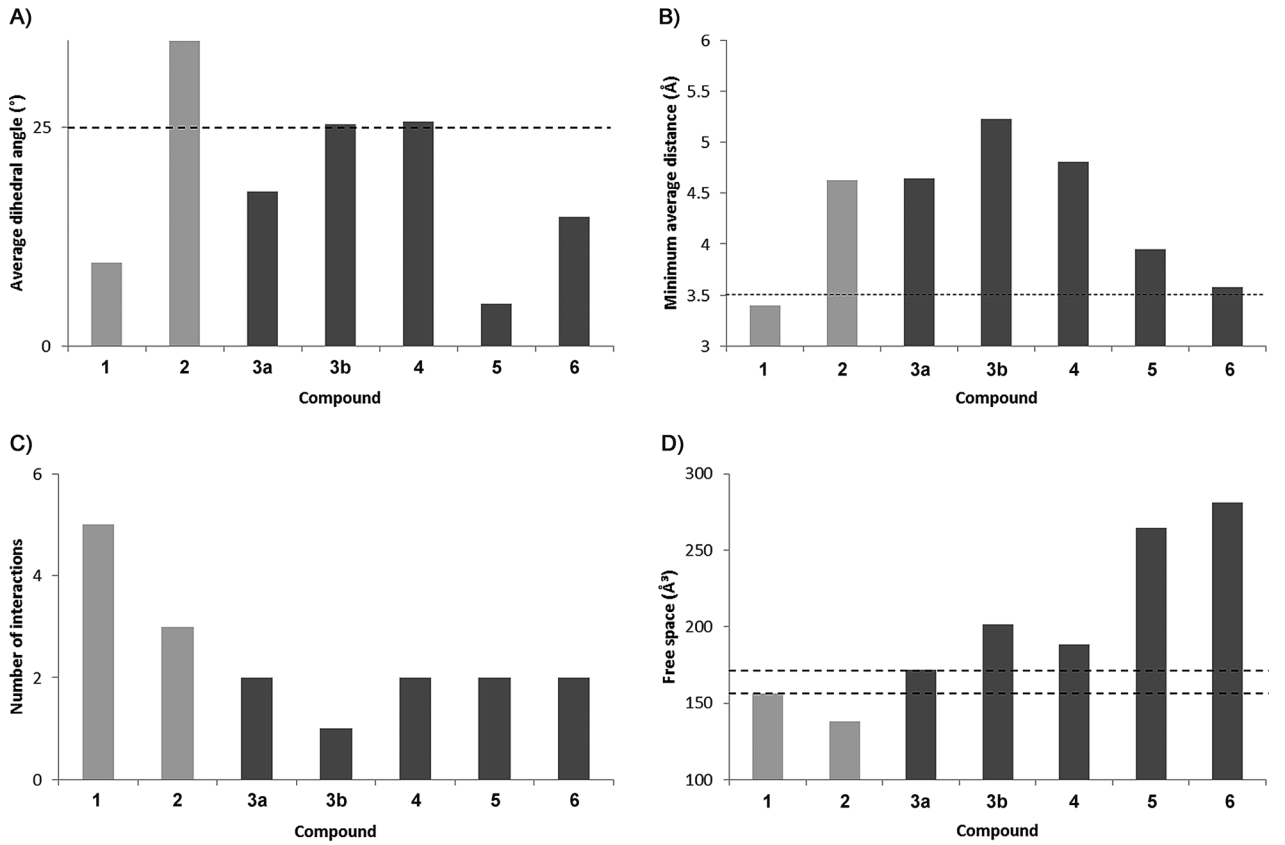

Figure 18. Evolution of several structural parameters for **1**–**6**. A) Anil maximum dihedral angle [°]. The black line corresponds to the 25° limit as discussed in the text. B) Minimum distance between molecules [Å]. The black line points out 3.5 Å intermolecular interactions. C) Number of interactions. D) Free space [Å]. Compound **3a** was taken as reference being the first photochromic molecule of the series with the lower free volume (160°). Light grey bars correspond to compounds presenting only thermochromism, dark grey bars represent photochromic species.

ism is observed when V_{free} exceeds 171 Å^3 (for **3**–**6**) whereas thermochromism is exclusively observed when $V_{free} \leq 153$ Å^3 (for **1** and **2**; Figure 18). This criterion is of interest for predicting optical properties. Indeed, considering the case of an "open" structure in which the anil molecules are packed in an open crystal lattice and reveal a large intramolecular distortion, photochromism is not necessarily observed if the new free volume condition is not fulfilled (like for **2**). This criterion is thus of major importance for a valuable prediction.

The flexibility of the local surroundings around the switching molecule may also explain the back reaction observed in photo-relaxation experiments for **4** and **5**. Indeed, during the thermal relaxation, only a fraction of the *trans*-keto form fully relaxes to the *cis*-keto form and the other fraction is trapped by the surrounding environment. This is seen after irradiation at $\lambda = 545$ nm of **5**; the *trans*→*cis* isomerisation proceeds but a fraction of the *cis*-keto form relaxes back to the *trans*-keto form, as noticed in Figure 19 for $t > 100$ min. Such a process, which occurs without relaxation to the *cis*-keto form, contrary to the spring-type effect,[20] is observed for the first time for an *N*-salicylidene derivative.

This phenomenon may be the signature of a cooperative mechanism that allows the stabilisation of the *trans*-keto form, usually considered as metastable at room temperature.[7] In this context, it is interesting to note that the *trans*-keto form is stabilised in **3a** and **3b** right after synthesis without any light irradiation. A stabilised *trans*-keto form was also observed in blend materials obtained by the insertion of *N*-salicylidene aniline sulfonate derivatives inside a polymer matrix (CopoC_6H), but no photochromism was observed in such materials.[13]

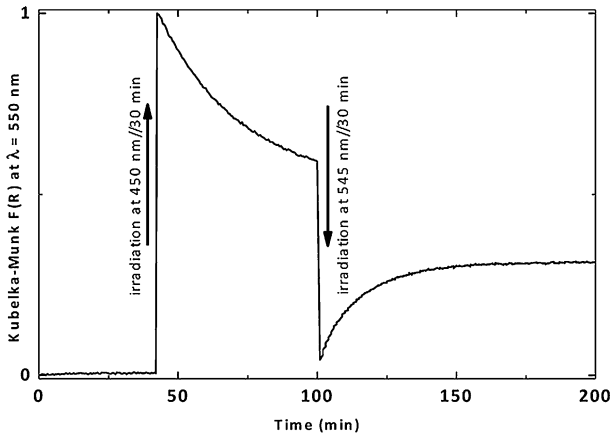

Figure 19. Time dependence of *F*(R) for **5** at $\lambda = 550$ nm showing the reversibility of the *cis*–*trans* isomerisation with irradiation cycle at $\lambda = 450$ and 545 nm, for 30 min.

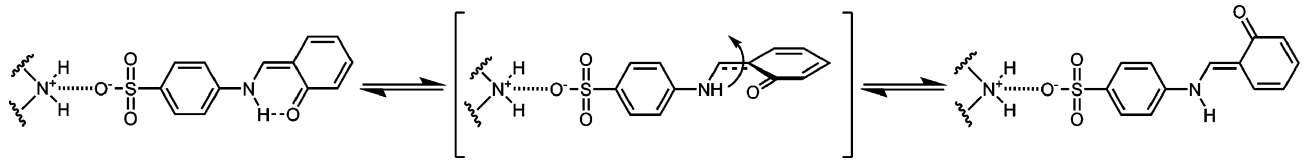

Scheme 5. Photo-isomerisation mechanism of *N*-salicylidene *p*-aniline sulfonate.

A different isomerisation mechanism is then proposed to explain the *cis–trans* isomerisation in a confined volume. Because the sulfonate interacts electrostatically with the ammonium cation, the ketone-bearing ring can rotate around with minimal packing restraint. The presence of intermolecular interaction and the alkyl surroundings may thus allow the stabilisation of the *trans*-keto form (Scheme 5).

Another point of interest concerns the stability of these molecules. All these compounds present a high thermal stability with a degradation temperature higher than 100 °C (283 °C for **3**, 284 °C for **1**[23b]). Interestingly, water molecules are observed inside the crystal structure of **1**·H_2O·MeOH, which shows that water is important for the crystallisation of this class of molecules, which are not that sensitive to hydrolysis compared with *N*-salicylidene aniline derivatives.[10] The high thermal stability, in addition to the resistance to hydrolysis, makes this substance class suitable for applications, for instance in optical storage and photochromic coatings.

Conclusion

Two approaches are usually followed to modify the optical properties of anils: 1) the variation of the nature of the substituent on the anil; and 2) variation of the surroundings, that is, by insertion in a given matrix. In this work, we carried out a systematic study of a series of well-characterised salts and even induced photochromism in a non-photochromic anion (**3**) without modifying its chemical nature, simply by modifying the counter-cation.

We have also shown that previous considerations on the importance of crystal packing and dihedral angles between aromatic rings[6,7] are no longer sufficient to account for optical properties, and that a new parameter considering the flexibility of the surrounding environment, represented by the available free space parameter in the crystal structure, needs to be taken into account. The flexibility of the local surroundings has also been considered to explain the spontaneous back reaction observed in photo-relaxation experiments as a consequence of the trapping of the anion in the *trans*-keto form.

This study also demonstrates that increasing the length of the lateral alkyl chain in diallylammonium derivatives favours a lamellar organisation, which was earlier suggested for poly(*N*,*N*-diallylamine-*alt*-maleic acid) copolymers.[31,32] The possibility of inducing photochromism by a slight change of the surroundings of an anil molecule, in addition to the ionic character of such anil derivatives, is promising for the incorporation of these charged derivatives into hybrid multifunctional materials and in co-crystal synthesis.[33]

Experimental Section

Starting materials

Solvents (HPLC grade methanol from Prolabo; [D_6]DMSO 99.98% D) and reagents (analytical grade sodium hydroxide from Fisher Scientific, salicylaldehyde 99%, 5-chlorosalicylaldehyde 98% from Acros Organics, sulfanilic acid from Sigma–Aldrich, 3-aminobenzenesulfonic acid from Fluka) were obtained commercially and used as received. The diallylamine derivatives were synthesised following previously reported procedures.[31]

Instrumentation

^{1}H and ^{13}C NMR spectra were recorded on a Bruker AC 300 MHz spectrometer with DMSO as internal standard. Infrared spectra were obtained on KBr disks by using an Equinox 55 instrument from Bruker. Diffuse reflectance spectra were recorded on a Varian Cary 5E spectrophotometer using PTFE as reference. Spectra were measured on pure solids to avoid matrix effects and presented as normalised Kubelka–Munk functions to allow meaningful comparisons. The reversibility of the *cis–trans* isomerisation was checked with a LOT-ORIEL 200 W high-pressure mercury arc lamp (LSN261). Ex situ irradiations were carried out for 30 min within a homemade chamber using appropriate filters (450 and 546 nm).

X-ray powder diffractograms were obtained using a Siemens D5000 X-ray diffractometer, with Cu radiation ($\lambda_{K\alpha}$ = 1.5418 Å).

Single-crystal data were collected on a MAR345 image plate, with $Mo_{K\alpha}$ radiation (Xenocs fox3D mirror) generated by a Rigaku UltraX 18 rotating anode. The reflections on the images were indexed and integrated using the CrysalisPro package (Agilent Technologies).[34] Data were scaled and corrected for absorption using the integrated Scale3 Abspack procedure. The structures were solved by direct methods (SHELXS-97)[35] and refined first isotropically and then anisotropically using SHELXL-97.[35] Hydrogen atoms were placed at calculated positions and refined in riding mode with respect to the parent atoms.

CCDC 1040108, 1040109, 1040110, 1040111, 1040112 and 1040113 contain the supplementary crystallographic data for this paper. These data can be obtained free of charge from The Cambridge Crystallographic Data Centre via www.ccdc.cam.ac.uk/data_request/cif.

Calculations

The molecular volume of each compound was calculated using the Molinspiration free toolkit (www.molinspiration.com).[36] The occupied volume was obtained by multiplying the volume of the anion and the cation by the number of monomers per aggregate.[37]

Synthesis

Synthesis of *N*-salicylidene *p*-aminobenzenesulfonate sodium (1): Sulfanilic acid (2.89 mmol) and NaOH (0.116 g, 2.89 mmol) were dissolved in MeOH (20 mL). Vigorous stirring was maintained until

complete solubilisation of the reagents. Salicylaldehyde (2.89 mmol) was then added dropwise to the solution. The temperature was increased to reflux (80 °C) and stirring was maintained overnight. A yellow solid was formed and then isolated by filtration. Purification was performed by recrystallisation from hot MeOH, which afforded yellow crystals. Yield: 66%. ^{1}H NMR ([D$_6$]DMSO): δ = 13.04 (s, 1H), 8.98 (s, 1H), 7.68 (d, $^3J_{H-H}$ = 8.43 Hz, 3H), 7.40 (m, 3H), 6.98 ppm (t, $^3J_{H-H}$ = 7.38 Hz, 2H); FTIR (KBr disk): $\tilde{\nu}$ = 1625 (C=N), 1134 (S=O), 730 (S–O$^-$), 651 cm^{-1} (C–S); elemental analysis calcd (%) for $C_{13}H_{10}NSO_4Na$: C 52.17, H 3.37, N 4.68; found: C 51.95, H 3.50, N 4.80.

Synthesis of *N*-salicylidene *p*-aminobenzenesulfonate salts: In a round flask, diallylamine derivative (5.52 mmol) was dissolved in MeOH (50 mL). Vigorous stirring at room temperature was applied and sulfanilic acid (6.07 equiv) was added when the diallylamine had completely dissolved. The stirring was maintained until no more acid was dissolved, which indicated the end of the reaction. The solution was filtered to remove the excess of acid and the solution was evaporated under vacuum. The product was then purified by recrystallisation from hot methanol. The sulfanilate of diallylammonium (1.41 mmol) was dissolved in MeOH (50 mL) in a round flask at room temperature. Salicylaldehyde (1.41 mmol) was added and vigorous stirring was maintained. The reaction was followed by ^{1}H NMR spectroscopy and then the solvent was evaporated under vacuum. The product was finally purified by recrystallisation in hot methanol.

***N*-Salicylidene *p*-aminobenzenesulfonate diallylammonium salt (2)**: M.p. 122 °C; ^{1}H NMR ([D$_6$]DMSO): δ = 8.97 (s, 1H), 8.74 (s, 2H), 7.66 (d, $^3J_{H-H}$ = 8.5 Hz, 3H), 7.37 (m, 3H), 6.97 (t, $^3J_{H-H}$ = 8 Hz, 2H), 5.87 (m, 2H), 5.42 (m, 4H), 3.56 ppm (d, $^3J_{H-H}$ = 5.9 Hz, 4H); ^{13}C NMR ([D$_6$]DMSO): δ = 163.66, 160.27, 147.97, 146.80, 133.34, 132.57, 128.86, 126.74, 122.61, 120.66, 119.28, 119.15, 116.57, 48.05 ppm; FTIR (KBr disk): $\tilde{\nu}$ = 1620 (C=N), 1120 (S=O), 728 (S–O$^-$), 639 cm^{-1} (C–S); elemental analysis calcd (%) for $C_{19}H_{22}N_2O_4S$: C 60.94, H 5.92, N 7.48; found: C 60.42, H 5.73, N 7.38.

***N*-Salicylidene *p*-aminobenzenesulfonate diallylhexylammonium salt (3)**: M.p. (TGA-TDA): 112 °C; degradation: 283 °C; ^{1}H NMR ([D$_6$]DMSO): δ = 8.97 (s, 1H), 7.66 (d, $^3J_{H-H}$ = 8.5 Hz, 3H), 7.37 (m, 3H), 6.97 (t, $^3J_{H-H}$ = 8 Hz, 2H), 5.93 (m, 2H), 5.53 (m, 4H), 3.73 (d, $^3J_{H-H}$ = 7 Hz, 4H), 2.97 (m, 2H), 1.61 (m, 2H), 1.25 (s, 6H), 0.85 ppm (m, 3H); ^{13}C NMR: δ = 170.68, 163.64, 160.27, 147.92, 133.34, 132.57, 127.00, 126.74, 125.31, 120.63, 119.28, 119.14, 116.55, 54.05, 51.44, 30.58, 25.58, 22.92, 21.81, 13.78 ppm; FTIR (KBr disk): $\tilde{\nu}$ = 1628 (C=N), 1167 (S=O), 727 (S–O$^-$), 667 cm^{-1} (C–S); elemental analysis calcd (%) for $C_{25}H_{34}N2O_4S$: C 65.47, H 7.47, N 6.11; found: C 65.21, H 7.37, N 5.89.

***N*-Salicylidene *p*-aminobenzenesulfonate diallyldecylammonium salt (4)**: M.p. 91 °C; ^{1}H NMR ([D$_6$]DMSO): δ = 8.97 (s, 1H), 7.66 (d, $^3J_{H-H}$ = 8.5 Hz, 3H), 7.37 (m, 3H), 6.97 (t, $^3J_{H-H}$ = 7.5 Hz, 2H), 5.93 (m, 2H), 5.53 (m, 4H), 3.73 (d, $^3J_{H-H}$ = 7 Hz, 4H), 2.96 (m, 2H), 1.61 (m, 2H), 1.23 (s, 14H), 0.84 ppm (m, 3H); ^{13}C NMR: δ = 170.68, 163.66, 160.31, 147.93, 132.60, 132.60, 127.04, 127.04, 126.76, 125.33, 120.65, 119.32, 116.59, 114.59, 54.09, 51.48, 37.00, 31.29, 28.88, 25.93, 23.00, 22.09, 21.00, 17.82, 13.96 ppm; FTIR (KBr disk): $\tilde{\nu}$ = 1617 (C=N), 1118 (S=O), 715 (S–O$^-$), 639 cm^{-1} (C–S); elemental analysis calcd (%) for $C_{29}H_{42}N_2O_4S$: C 67.67, H 8.22, N 5.44; found: C 67.46, H 8.57, N 5.36.

***N*-Salicylidene *p*-aminobenzenesulfonate diallyldodecylammonium salt (5)**: M.p. 68 °C; ^{1}H NMR ([D$_6$]DMSO): δ = 8.97 (s, 1H), 7.66 (d, $^3J_{H-H}$ = 8.5 Hz, 3H), 7.37 (m, 3H), 6.97 (t, $^3J_{H-H}$ = 7.6 Hz, 2H), 5.93 (m, 2H), 5.53 (m, 4H), 3.73 (d, $^3J_{H-H}$ = 7 Hz, 4H), 2.96 (m, 2H), 1.60 (m, 2H), 1.22 (s, 18H), 0.84 ppm (m, 3H); ^{13}C NMR: δ = 163.63, 160.27, 146.89, 133.33, 132.57, 126.74, 125.28, 120.63, 119.28, 116.55, 54.05, 51.44, 44.30, 42.45, 41.65, 41.15, 31.27, 28.98, 28.89, 28.41, 25.90, 22.96, 22.07, 13.93 ppm; FTIR (KBr disk): $\tilde{\nu}$ = 1617 (C=N), 1117 (S=O), 714 (S–O$^-$), 641 cm^{-1} (C–S); elemental analysis calcd (%) for $C_{31}H_{46}N_2O_4S$: C 68.60, H 8.54, N 5.16; found: C 68.42, H 8.90, N 5.02.

***N*-Salicylidene *p*-aminobenzenesulfonate diallyloctadecylammonium salt (6)**: M.p. 76 °C; ^{1}H NMR ([D$_6$]DMSO): δ = 8.97 (s, 1H), 7.66 (d, $^3J_{H-H}$ = 8.5 Hz, 3H), 7.37 (m, 3H), 6.97 (t, $^3J_{H-H}$ = 7.6 Hz, 2H), 5.93 (m, 2H), 5.53 (m, 4H), 3.72 (d, $^3J_{H-H}$ = 6.7 Hz, 4H), 2.95 (m, 2H), 1.60 (m, 2H), 1.22 (s, 30H), 0.84 ppm (m, 3H); ^{13}C NMR: δ = 163.67, 160.33, 146.96, 133.36, 132.63, 126.79, 120.67, 119.18, 116.60, 54.11, 31.31, 29.07, 28.95, 25.96, 22.12, 13.97, 7.54 ppm; FTIR (KBr disk): $\tilde{\nu}$ = 1617 (C=N), 1118 (S=O), 717 (S–O$^-$), 642 cm^{-1} (C–S); elemental analysis calcd (%) for $C_{37}H_{58}N_2O_4S$: C 70.89, H 9.32, N 4.47; found: C 71.00, H 9.80, N 4.21.

Acknowledgements

This work was funded by the ARC Académie Louvain program (08/13-010), the Fonds National de la Recherche Scientifique-FNRS and the COST MP1202. We also thank the Fonds pour la Formation à la Recherche dans l'Industrie et dans l'Agriculture for a doctoral scholarship allocated to P.-L.J.

Keywords: isomerization · molecular devices · photochromism · tautomerism · thermochromism

[1] a) G. H. Brown, *Photochromism*, Wiley, New York, **1971**; b) J. C. Crano, R. J. Guglielmetti, *Organic Photochromic and Thermochromic compounds*, Plenum, New York, **1998**; c) M. Irie, *Chem. Rev.* **2000**, *100*, 1683; d) B. L. Feringa, *Acc. Chem. Res.* **2001**, *34*, 504; e) H. Dürr, Bouas-Laurent, *Photochromism: Molecules and Systems*, 2nd ed., Elsevier, Amsterdam, **2003**.

[2] W. A. Velema, W. Szymanski, B. L. Feringa, *J. Am. Chem. Soc.* **2014**, *136*, 2178.

[3] M. Natali, S. Giordani, *Chem. Soc. Rev.* **2012**, *41*, 4010.

[4] I. O. Staehle, B. Rodriguez-Molina, S. I. Khan, M. A. Garcia-Garibay, *Cryst. Growth Des.* **2014**, *14*, 3667.

[5] a) T. Fujiwara, J. Harada, K. Ogawa, *J. Phys. Chem. B* **2004**, *108*, 4035; b) E. Hadjoudis, *Mol. Eng.* **1995**, *5*, 301; c) E. Hadjoudis, I. M. Mavridis, *Chem. Soc. Rev.* **2004**, *33*, 579; d) E. Hadjoudis, S. D. Chatziefthimiou, I. M. Mavridis, *Curr. Org. Chem.* **2009**, *13*, 269.

[6] a) M. D. Cohen, G. M. J. Schmidt, *J. Phys. Chem.* **1962**, *66*, 2442; b) M. D. Cohen, G. M. J. Schmidt, S. Flavian, *J. Chem. Soc.* **1964**, 2041; c) M. D. Cohen, Y. Hirshberg, G. M. J. Schmidt, *J. Chem. Soc.* **1964**, 2051; d) M. D. Cohen, Y. Hirshberg, G. M. J. Schmidt, *J. Chem. Soc.* **1964**, 2060; e) J. Bregman, L. Leiserowitz, G. M. J. Schmidt, *J. Chem. Soc.* **1964**, 2068; f) M. D. Cohen, S. Flavian, *J. Chem. Soc. B* **1967**, 317; g) M. D. Cohen, S. Flavian, *J. Chem. Soc. B* **1967**, 321; h) M. D. Cohen, S. Flavian, L. Leiserowitz, *J. Chem. Soc. B* **1967**, 329; i) M. D. Cohen, S. Flavian, *J. Chem. Soc. B* **1967**, 334; j) M. D. Cohen, *J. Chem. Soc. B* **1968**, 373.

[7] E. Hadjoudis, M. Vittorakis, I. Moustakali-Mavridis, *Tetrahedron* **1987**, *43*, 1345.

[8] a) F. Robert, A. D. Naik, B. Tinant, R. Robiette, Y. Garcia, *Chem. Eur. J.* **2009**, *15*, 4327; b) F. Robert, P.-L. Jacquemin, B. Tinant, Y. Garcia, *CrystEngComm* **2012**, *14*, 4396.

[9] L. Z. Zhang, Y. Xiong, P. Cheng, G.-Q. Tang, D.-Z. Liao, *Chem. Phys. Lett.* **2002**, *358*, 278.

[10] M. Ziolek, I. Sobczak, *J. Inclusion Phenom. Macrocyclic Chem.* **2009**, *63*, 211.

[11] E. Hadjoudis, A. B. Bourlinos, D. Petridis, *J. Inclusion Phenom. Macrocyclic Chem.* **2002**, *42*, 275.

[12] E. Hadjoudis, V. Verganelakis, C. Trapalis, G. Kordas, *Mol. Eng.* **1999**, *8*, 459.

[13] P.-L. Jacquemin, Y. Garcia, M. Devillers, *J. Mater. Chem. C* **2014**, *2*, 1815.

[14] a) E. Hadjoudis, T. Dziembowska, Z. Rozwadowski, *J. Photochem. Photobiol. A* **1999**, *128*, 97; b) E. Hadjoudis, K. Yannakopoulo, S. D. Chatziefthimiou, A. Paulidou, I. M. Mavridis, *J. Photochem. Photobiol. A* **2011**, *217*, 293.
[15] a) T. Haneda, M. Kawano, T. Kojima, M. Fujita, *Angew. Chem. Int. Ed.* **2007**, *46*, 6643; *Angew. Chem.* **2007**, *119*, 6763; b) Y. Inokuma, M. Kawano, M. Fujita, *Nat. Chem.* **2011**, *3*, 349.
[16] a) T. Kawato, H. Koyama, H. Kamatomi, K. Yonetani, H. Matsushita, *Chem. Lett.* **1994**, 665; b) T. Kawato, K. Amimoto, H. Maeda, H. Koyama, H. Kanatomi, *Mol. Cryst. Liq. Cryst.* **2000**, *345*, 57.
[17] I. Casades, M. Alvaro, H. Garcia, M. N. Pillai, *Eur. J. Org. Chem.* **2002**, 2074.
[18] a) M. Gil, M. Ziolek, J. A. Organero, A. Douhal, *J. Phys. Chem. C* **2010**, *114*, 9554; b) B. Cohen, S. Wang, J. A. Organero, L. F. Campo, F. Sanchez, A. Douhal, *J. Phys. Chem. C* **2010**, *114*, 6281.
[19] M. Sliwa, P. Naumov, H. J. Choi, Q.-T. Nguyen, B. Debus, S. Delbaere, C. Ruckebush, *ChemPhysChem* **2011**, *12*, 1669.
[20] F. Robert, A. D. Naik, F. Hidara, B. Tinant, R. Robiette, J. Wouters, Y. Garcia, *Eur. J. Org. Chem.* **2010**, 621.
[21] F. Robert, B. Tinant, R. Clérac, P.-L. Jacquemin, Y. Garcia, *Polyhedron* **2010**, *29*, 2739.
[22] Y. Garcia, F. Robert, A. D. Naik, G. Zhou, B. Tinant, K. Robeyns, S. Michotte, L. Piraux, *J. Am. Chem. Soc.* **2011**, *133*, 15850 – 15853.
[23] a) F. Robert, A. D. Naik, Y. Garcia, *J. Phys. Conf. Ser.* **2010**, *217*, 012031; b) F. Robert, A. D. Naik, B. Tinant, Y. Garcia, *Inorg. Chim. Acta* **2012**, *380*, 104.
[24] X. R. Wang, J. Lu, D. Yan, M. Wei, D. G. Evans, X. Duan, *Chem. Phys. Lett.* **2010**, *493*, 333.
[25] P.-L. Jacquemin, K. Robeyns, M. Devillers, Y. Garcia, *Chem. Commun.* **2014**, *50*, 649.
[26] P. Guionneau, *Dalton Trans.* **2014**, *43*, 382.
[27] D. A. Safin, M. G. Babashkina, K. Robeyns, M. Bolte, Y. Garcia, *CrystEngComm* **2014**, *16*, 7053.
[28] M. Juribasic, N. Bregovic, V. Stilinovic, V. Tomisic, M. Cindric, P. S Ket, J. Plavec, M. Rubcic, K. Uzarevic, *Chem. Eur. J.* **2014**, *20*, 17333.
[29] D. A. Safin, K. Robeyns, Y. Garcia, *CrystEngComm* **2012**, *14*, 5523 – 5529.
[30] a) P. Köberle, A. Laschewsky, *Makromol. Chem.* **1992**, *193*, 1815; b) P. Koeberle, A. Laschewsky, *Macromolecules* **1994**, *27*, 2165.
[31] F. Rullens, M. Devillers, A. Laschewsky, *Macromol. Chem. Phys.* **2004**, *205*, 1155.
[32] a) F. Rullens, N. Deligne, A. Laschewsky, M. Devillers, *J. Mater. Chem.* **2005**, *15*, 1668; b) F. Rullens, M. Devillers, A. Laschewsky, *J. Mater. Chem.* **2004**, *14*, 3421; c) F. Rullens, A. Laschewsky, M. Devillers, *Chem. Mater.* **2006**, *18*, 771; d) G. Raj, C. Swalus, A. Guillet, M. Devillers, B. Nysten, E. M. Gaigneaux, *Langmuir* **2013**, *29*, 4388.
[33] K. M. Hutchins, S. Dutta, B. P. Loren, L. R. MacGillivray, *Chem. Mater.* **2014**, *26*, 3042.
[34] Oxford Diffraction Data collection and data reduction, Version 1.171.35.19 (.**1** – **5**); Version 1.171.36.21 (6).
[35] G. M. Sheldrick, *Acta Crystallogr. A* **2008**, *64*, 112.
[36] Molinspiration Property Calculation Service, www.molinspiration.com.
[37] K. E. D. Coan, B. K. Shoichet, *J. Am. Chem. Soc.* **2008**, *130*, 9606.

Received: December 19, 2014
Published online on March 12, 2015